

Splitting methods for nonlinear Dirac equations with thirring type interaction in the nonrelativistic limit regime

Patrick Krämer, Katharina Schratz, Xiaofei Zhao

CRC Preprint 2018/33, November 2018

KARLSRUHE INSTITUTE OF TECHNOLOGY

CRC 1173



Wave
phenomena

Participating universities



Universität Stuttgart

EBERHARD KARLS
UNIVERSITÄT
TÜBINGEN



Funded by

DFG

ISSN 2365-662X

Splitting Methods for Nonlinear Dirac Equations with Thirring type Interaction in the Nonrelativistic Limit Regime

Patrick Krämer*, Katharina Schratz

Karlsruhe Institute of Technology, Faculty of Mathematics, 76131 Karlsruhe, Germany

Xiaofei Zhao

School of Mathematics and Statistics, Wuhan University, Wuhan 430072, China

Abstract

Nonlinear Dirac equations describe the motion of relativistic spin- $\frac{1}{2}$ particles in presence of external electromagnetic fields, modelled by an electric and magnetic potential, and taking into account a nonlinear particle self-interaction. In recent years, the construction of numerical splitting schemes for the solution of these systems in the nonrelativistic limit regime, i.e., the speed of light c formally tending to infinity, has gained a lot of attention. In this paper, we consider a nonlinear Dirac equation with Thirring type interaction, where in contrast to the case of the Soler type nonlinearity a classical two-term splitting scheme cannot be straightforwardly applied. Thus, we propose and analyze a three-term Strang splitting scheme which relies on splitting the full problem into the free Dirac subproblem, a potential subproblem, and a nonlinear subproblem, where each subproblem can be solved exactly in time. Moreover, our analysis shows that the error of our scheme improves from $\mathcal{O}(\tau^2 c^4)$ to $\mathcal{O}(\tau^2 c^3)$ if the magnetic potential in the system vanishes. Furthermore, we propose an efficient limit approximation scheme for solving nonlinear Dirac systems in the nonrelativistic limit regime $c \gg 1$ which allows errors of order $\mathcal{O}(c^{-1})$ without any c -dependent time step restriction.

Keywords: Dirac equation, time integration, splitting methods, error estimates, highly-oscillatory, nonrelativistic limit

*Corresponding author

Email addresses: kraemer.patrick.kit@outlook.com (Patrick Krämer),
katharina.schratz@kit.edu (Katharina Schratz), zhxfnus@gmail.com (Xiaofei Zhao)

1. Introduction

Dirac equations describe the motion of relativistic spin- $\frac{1}{2}$ particles, such as for example electrons ([11, 26]). In this paper, we address the construction and analysis of a splitting scheme for solving Dirac equations with Thirring type nonlinear self-interaction ([27]). We thus consider

$$i\partial_t\Psi = -ic\sum_{j=1}^d\alpha_j\partial_j\Psi + c^2\beta\Psi + \left(\phi - \sum_{j=1}^d\alpha_jA_j\right)\Psi + \lambda(\Psi\cdot\beta\bar{\Psi})\beta\Psi \quad (1)$$

$$\Psi(0,x) = \Psi^0(x) \in \mathbb{C}^4, \quad c \geq 1, \quad \lambda \geq 0, \quad \alpha_j, \beta \in \mathbb{C}^{4 \times 4}, \quad j = 1, \dots, d \quad (\text{see (2)})$$

in $d = 1, 2, 3$ spatial dimensions equipped with periodic boundary conditions on the d -dimensional torus $\mathbb{T}^d = [-\pi, \pi]^d$ for finite times $t \in [0, T]$, with solution $\Psi(t, x) \in \mathbb{C}^4$. In the latter equation the influence of an external electromagnetic field is modelled through a term involving an electric scalar potential $\phi(t, x) \in \mathbb{R}$ and a magnetic vector potential $\mathcal{A}(t, x) = (A_1(t, x), \dots, A_d(t, x))^T$, where the electric field E and the magnetic field B are given as $E = -\nabla\phi - c^{-1}\partial_t\mathcal{A}$ and $B = \nabla \times \mathcal{A}$. The term $\lambda(\Psi\cdot\beta\bar{\Psi})\beta\Psi$ models the Thirring type interaction ([27]). The parameter $c := c_0/v_p$ in the equation describes the relation between the speed of light c_0 and the velocity of the particle v_p . In the relativistic regime where the particle velocity is close to the speed of light, i.e., $v_p \lesssim c_0$, this parameter $c \gtrsim 1$ is small. On the other hand, in the so-called nonrelativistic limit regime the particle velocity is very small compared to the speed of light, i.e., $v_p \ll c_0$, and the parameter $c \gg 1$ becomes very large as $c \rightarrow \infty$, which triggers high oscillations in the solution. One of the main challenges in constructing numerical schemes for solving nonlinear Dirac equations (1) lies in capturing this highly oscillatory nature of the solution in the so-called nonrelativistic limit regime $c \gg 1$.

In recent years, many multiscale methods have been developed for solving the Dirac equations in the nonrelativistic limit regime ([2, 10, 20]). These methods either rely on some pre-knowledge of the solution or are sophisticated for practical use. Moreover, splitting methods for Dirac equations in relativistic and nonrelativistic regimes have recently gained a lot of attention ([3–5, 16, 19]). In [4], the authors construct and analyze a Strang splitting scheme (TSFP scheme) for the numerical solution of the nonlinear Dirac equation (1) with the Soler type interaction ([25]). Applying it with time step size τ , it allows error bounds of order $\mathcal{O}(\tau^2c^4)$ ([4, Theorem 4.3]). Under a particular choice of the time step $\tau = 2\pi/(c^2N)$ for arbitrary number $N \in \mathbb{N}$ the authors show an improved error bound of order $\mathcal{O}(\tau^2c^2)$ ([4, Theorem 4.4]).

In this paper, we introduce and analyze a three-term Strang splitting scheme for the nonlinear Dirac equation (1) which contains the Thirring type interaction. For the spatial discretization, we choose Fourier pseudospectral techniques ([12, 21]). In the following we call the latter Extended Time Splitting Fourier Pseudospectral (ETSFP) Scheme. In this case the two-term splitting which was considered and analyzed in [4] could not be applied. Our new three-term ETSFP scheme allows error bounds of order $\mathcal{O}(\tau^2(c^4K_{\mathcal{A}} + c^3K_1))$. Thereby, if we assume that the vector potential vanishes, i.e., if $\mathcal{A} \equiv 0$, the constant $K_{\mathcal{A}} = 0$ vanishes and the error bound improves to $\mathcal{O}(\tau^2(c^3K_1))$. These theoretical results are collected in Theorem 1. Moreover, our numerical results in Section 6 suggest

that our bounds can be further improved to $\mathcal{O}(\tau^2 c^2)$ under the time step restriction $\tau \lesssim c^{-2}$ (see [4, Theorem 4.4] for the case of the Soler type interaction). Note that due to the theoretical error bounds of order $\mathcal{O}(\tau^2 c^4)$ this is a natural requirement on the time step in order to obtain convergence of the scheme.

Furthermore, the numerical results in Section 6 show that the error behaviour of our scheme significantly improves if the vector potential vanishes, i.e., $\mathcal{A} \equiv 0$, and if we assume higher regularity of the data than required in Theorem 1.

Secondly, we numerically compare the solutions, obtained with our splitting scheme, to an asymptotic approximation in the nonrelativistic limit $c \rightarrow \infty$, which allows analytic error bounds of order $\mathcal{O}(c^{-1})$. The latter reduces the task to solving a c -independent system of nonlinear Schrödinger equations (see results for the case of Klein–Gordon, Dirac, Maxwell–Klein–Gordon and Maxwell–Dirac equations in [6–9, 23, 24] (analytical) and [13, 18, 19] (numerical)).

The $\mathbb{C}^{4 \times 4}$ Dirac matrices α_j , $j = 1, 2, 3$ and β in (1) are given as

$$\alpha_j = \begin{pmatrix} \mathbf{0}_2 & \sigma_j \\ \sigma_j & \mathbf{0}_2 \end{pmatrix}, \quad \beta = \begin{pmatrix} \mathcal{I}_2 & \mathbf{0}_2 \\ \mathbf{0}_2 & -\mathcal{I}_2 \end{pmatrix}, \quad \text{for } j = 1, \dots, 3 \quad (2)$$

involving the Pauli matrices

$$\sigma_1 = \begin{pmatrix} 0 & 1 \\ 1 & 0 \end{pmatrix}, \quad \sigma_2 = \begin{pmatrix} 0 & -i \\ i & 0 \end{pmatrix}, \quad \sigma_3 = \begin{pmatrix} 1 & 0 \\ 0 & -1 \end{pmatrix},$$

where $\mathbf{0}_N$ and \mathcal{I}_N denote the $N \times N$ zero and identity matrix, respectively. Note that for $z \in \mathbb{C}$ the expression \bar{z} denotes the complex conjugate of z . Furthermore, note that $u \cdot v := \sum_{j=1}^N u_j v_j$ denotes the standard Euclidean inner product of vectors $u, v \in \mathbb{C}^N$.

For sake of simpler notion, in the following we abbreviate

$$\begin{aligned} \mathcal{H}\Psi &:= -ic \sum_{j=1}^d \alpha_j \partial_j \Psi + c^2 \beta \Psi, & \mathcal{V}[\phi, \mathcal{A}]\Psi &:= \left(\phi - \sum_{j=1}^d \alpha_j A_j \right) \Psi \\ \mathcal{N}(\Psi) &:= \lambda(\Psi \cdot \beta \bar{\Psi}) \beta \Psi, \end{aligned} \quad (3)$$

such that we can compactly write (1) as

$$i \partial_t \Psi = \mathcal{H}\Psi + \mathcal{V}[\phi, \mathcal{A}]\Psi + \mathcal{N}(\Psi), \quad \Psi(0, x) = \Psi^0(x) \in \mathbb{C}^4. \quad (4)$$

We call the operator \mathcal{H} the free Dirac operator (see also [26]).

2. Time Splitting Schemes for Dirac Equations

2.1. The case of the Soler type interaction

In [3] the authors proposed and analyzed a Strang splitting scheme (Time Splitting Fourier Pseudospectral scheme¹, TSFP) for numerically solving the Dirac equation with

¹Fourier Pseudospectral discretization in space, cf. [12]

Soler type nonlinearity ([25])

$$i\partial_t\Psi = \mathcal{H}\Psi + \mathcal{V}[\phi, \mathcal{A}]\Psi + \mu|\Psi|^2\Psi, \quad \mu \in \mathbb{R}. \quad (5)$$

The idea is thereby based on splitting the equation into the two subproblems (see also [12, 22] for Nonlinear Schrödinger equations)

$$i\partial_t\Psi = \mathcal{H}\Psi, \quad \Psi(0) = \Psi^0 \quad \text{and} \quad i\partial_t\Psi = \mathcal{V}[\phi, \mathcal{A}]\Psi + \mathcal{S}(\Psi), \quad \Psi(0) = \Psi^0,$$

where $\mathcal{S}(\Psi) := \mu|\Psi|^2\Psi$ denotes the nonlinear Soler type interaction. Note that we can solve the first subproblem exactly in time by considering it in Fourier space. Thanks to the relation $\partial_t|\Psi|^2 = 0$ in the second subproblem, the latter can be solved exactly in time as well. We denote their solution operators (their *exact flows*) by $\varphi_{\mathcal{H}}^t$ and $\varphi_{\mathcal{V}+\mathcal{S}}^t$, respectively. To obtain an approximation to the full system, these flows are then combined as follows:

$$\Psi^{n+1} = \varphi_{\mathcal{H}}^{\tau/2} \circ \varphi_{\mathcal{V}+\mathcal{S}}^{\tau} \circ \varphi_{\mathcal{H}}^{\tau/2}(\Psi^n) \approx \Psi(t_{n+1}), \quad t_n = n\tau, \quad n = 0, 1, 2, \dots, \quad (6)$$

where $0 < \tau \leq 1$ is a small time step size. The resulting numerical solution Ψ^{n+1} is then a second order in time approximation to the exact solution $\Psi(t_{n+1})$ at time t_{n+1} .

However, replacing in (5) the Soler interaction $\mathcal{S}(\Psi)$ by our Thirring interaction $\mathcal{N}(\Psi)$ such a two term splitting idea will not apply. This challenge is discussed in the next section. For an extensive overview on splitting methods for ordinary and partial differential equations, we refer to [14] and [12, 17, 21, 22], respectively.

2.2. The Challenges in the Case of Thirring type Nonlinearity

In this section, we outline why the TSFP method (6) (cf. [4]) can not be straightforwardly extended to the nonlinear setting (4) with $\lambda > 0$, and discuss the additional challenge that arises. Following the strategy of the previous section, we split the Dirac equation (4) with Thirring type nonlinearity into the subproblems $i\partial_t\Psi = \mathcal{H}\Psi$ and

$$i\partial_t\Psi = \mathcal{V}[\phi, \mathcal{A}]\Psi + \mathcal{N}(\Psi) = \left(\phi - \sum_{j=1}^d \alpha_j A_j \right) \Psi + \lambda(\Psi \cdot \beta \bar{\Psi})\beta\Psi, \quad (7)$$

with given initial data each. A simple calculation shows that within subproblem (7)

$$\partial_t(\Psi(t) \cdot \beta \bar{\Psi}(t)) = -2 \sum_{j=1}^d A_j(t) \operatorname{Im}(\alpha_j \Psi(t) \cdot \beta \bar{\Psi}(t)) \neq 0.$$

Therefore, in contrast to Section 2.1 we are not able to write down an explicit expression for the exact flow $\varphi_{\mathcal{V}+\mathcal{N}}^t(\Psi(0))$ of the nonlinear subproblem (7). In view of practical implementation, we thus have to apply an additional approximation to $\varphi_{\mathcal{V}+\mathcal{N}}^t(\Psi(0))$ in order to compute the Strang splitting iteration

$$\Psi^{n+1} = \varphi_{\mathcal{H}}^{\tau/2} \circ \varphi_{\mathcal{V}+\mathcal{N}}^{\tau} \circ \varphi_{\mathcal{H}}^{\tau/2}(\Psi^n) \approx \Psi(t_{n+1}) \quad (8)$$

for $t_n = n\tau$, $n = 0, 1, 2, \dots$. More precisely, we have to approximate $\varphi_{\mathcal{V}+\mathcal{N}}^{\tau}$ by a suitable numerical scheme, which preserves the second order global convergence of the Strang splitting scheme (8). We present the resulting three-term Strang splitting scheme in the next section.

2.3. The extended TSFP (ETSFP) scheme for the nonlinear Dirac equation

In this section, we present a three-term splitting scheme for the nonlinear Dirac equation (4). A detailed, rigorous global error analysis of this ETSFP scheme will be given later on in Section 4 by interpreting it as a perturbation of the 2-term splitting scheme (8).

As a first step in the construction of the scheme, we split the full problem (4) into the free Dirac subproblem

$$i\partial_t\Psi = \mathcal{H}\Psi = \left(-ic\sum_{j=1}^d\alpha_j\partial_j + c^2\beta\right)\Psi, \quad \Psi(0) = \Psi^0, \quad (9a)$$

the potential subproblem

$$i\partial_t\Psi = \mathcal{V}[\phi, \mathcal{A}]\Psi = \left(\phi - \sum_{j=1}^d\alpha_j A_j\right)\Psi, \quad \Psi(0) = \Psi^0, \quad (9b)$$

and the nonlinear subproblem

$$i\partial_t\Psi = \mathcal{N}(\Psi) = \lambda(\Psi \cdot \beta\bar{\Psi})\beta\Psi, \quad \Psi(0) = \Psi^0. \quad (9c)$$

Note that the exact flows $\varphi_{\mathcal{H}}^t$, $\varphi_{\mathcal{V}}^t$ and $\varphi_{\mathcal{N}}^t$ of these subproblems can be computed exactly in time. For details on practical implementation of these flows, see Section 3.1 and [3, Appendix 3].

In order to globally obtain second order convergence of our scheme, we approximate the exact flow $\varphi_{\mathcal{V}+\mathcal{N}}^\tau$ of (7) in (8) through another Strang splitting scheme applied to (7). More precisely, we take

$$\Phi_{\mathcal{V}+\mathcal{N}}^\tau(\Psi^0) := \varphi_{\mathcal{N}}^{\tau/2} \circ \varphi_{\mathcal{V}}^\tau \circ \varphi_{\mathcal{N}}^{\tau/2}(\Psi^0) \approx \varphi_{\mathcal{V}+\mathcal{N}}^\tau(\Psi^0). \quad (10)$$

Plugging in (10) into (8) results in the final extended TSFP (ETSFP) scheme

$$\Psi^{n+1} = \Phi_{ETSFP}^\tau(\Psi^n) = \varphi_{\mathcal{H}}^{\tau/2} \circ \varphi_{\mathcal{N}}^{\tau/2} \circ \varphi_{\mathcal{V}}^\tau \circ \varphi_{\mathcal{N}}^{\tau/2} \circ \varphi_{\mathcal{H}}^{\tau/2}(\Psi^n) \approx \Psi(t_{n+1}). \quad (11)$$

The flows $\varphi_{\mathcal{H}}^\tau$, $\varphi_{\mathcal{N}}^\tau$ and $\varphi_{\mathcal{V}}^\tau$ are defined in (12), (14) and (15), respectively.

3. A priori bounds

In the following, let $\|u\|_r^2 = \sum_{k \in \mathbb{Z}^d} (1 + |k|)^{2r} |\widehat{u}_k|^2$ denote the classical Sobolev norm for $u \in H^r(\mathbb{T}^d)$, where \widehat{u}_k , $k \in \mathbb{Z}^d$ denote the corresponding Fourier coefficients of u .

Note that we define the $(H^r)^m$ -norm of a vector valued function $U : \mathbb{T}^d \rightarrow \mathbb{C}^m$, $U(x) = (u_1(x), \dots, u_m(x))^\top$ with \mathbb{T}^d -periodic components u_ℓ , $\ell = 1, \dots$ as

$$\|U\|_{(H^r)^m}^2 := \|u_1\|_r^2 + \dots + \|u_m\|_r^2,$$

where for sake of simplicity we may also write $\|U\|_r = \|U\|_{(H^r)^m}$ instead. Moreover, we write $\widehat{U}_k(t) = \left(\widehat{(u_1)_k}(t), \dots, \widehat{(u_m)_k}(t)\right)^\top$ and denote by $U \cong \widehat{U}_k$, $k \in \mathbb{Z}^d$ the representation of U in Fourier space by its coefficients \widehat{U}_k . Next, we set up stability bounds for the flows $\varphi_{\mathcal{H}}^t$, $\varphi_{\mathcal{V}}^t$ and $\varphi_{\mathcal{N}}^t$.

3.1. Stability bounds for the subproblems

The free Dirac subproblem: The free Dirac operator $\mathcal{H}\Psi$ in the nonlinear equation (4) reads

$$\mathcal{H}\Psi = -ic \sum_{j=1}^d \alpha_j \partial_j \Psi + c^2 \beta \Psi \cong \widehat{\mathcal{H}}_k \widehat{\Psi}_k, \quad k \in \mathbb{Z}^d$$

with $\widehat{\mathcal{H}}_k \in \mathbb{C}^{4 \times 4}$ denoting the k -th Fourier symbol of \mathcal{H} .

Exploiting that $\widehat{\mathcal{H}}_k$ is orthogonally diagonalizable with real eigenvalues $\pm c\sqrt{|k|^2 + c^2}$ (for details on the practical implementation, see for example [3, Appendix 3], [26, Chapter 1.4] and [19, Chapter 5.2.1]), we easily verify that the exact flow

$$\varphi_{\mathcal{H}}^{\tau}(\Psi^0) = \exp(-i\tau\mathcal{H})\Psi^0 \cong \exp(-i\tau\widehat{\mathcal{H}}_k)\widehat{\Psi}_k^0, \quad k \in \mathbb{Z}^d \quad (12)$$

of the free Dirac problem (9a) is an isometry in H^r , i.e.,

$$\|\varphi_{\mathcal{H}}^{\tau}(\Psi^0)\|_r = \|\Psi^0\|_r. \quad (13)$$

In particular, for different initial values Ψ^0 and $\widetilde{\Psi}^0$, we obtain the stability bound

$$\left\| \varphi_{\mathcal{H}}^{\tau}(\Psi^0) - \varphi_{\mathcal{H}}^{\tau}(\widetilde{\Psi}^0) \right\|_r = \left\| \Psi^0 - \widetilde{\Psi}^0 \right\|_r.$$

The potential and nonlinear subproblem: Considering the nonlinear subproblem (9c), we observe that thanks to $(\Psi(t, x) \cdot \beta \overline{\Psi}(t, x)) \in \mathbb{R}$ and $\beta^2 = \mathcal{I}_4$, and thanks to the product rule, we have the relation

$$\partial_t (\Psi \cdot \beta \overline{\Psi}) = -i\lambda(\Psi \cdot \beta \overline{\Psi})\beta\Psi \cdot \beta\overline{\Psi} + \Psi \cdot \beta (+i\lambda(\Psi \cdot \beta \overline{\Psi})\beta\overline{\Psi}) \equiv 0,$$

which allows us to compute the corresponding exact flow as

$$\varphi_{\mathcal{N}}^{\tau}(\Psi^0(x)) = \text{diag} \left(e^{-i\tau\lambda(\Psi^0(x) \cdot \beta \overline{\Psi}^0(x))} \mathcal{I}_2, e^{+i\tau\lambda(\Psi^0(x) \cdot \beta \overline{\Psi}^0(x))} \mathcal{I}_2 \right) \Psi^0(x). \quad (14)$$

Similarly, the flow of the potential subproblem (9b) is given through

$$\varphi_{\mathcal{V}}^{\tau}(\Psi(t, x)) = e^{-i \int_t^{t+\tau} \mathcal{V}[\phi(s, x), \mathcal{A}(s, x)] ds} \Psi(t, x). \quad (15)$$

For practical implementation issues, we approximate the integral via the second order trapezoidal rule [3, Appendix 3] in order to obtain the numerical flow

$$\Phi_{\mathcal{V}}^{\tau}(\Psi(t, x)) = e^{-i \frac{\tau}{2} (\mathcal{V}(t, x) + \mathcal{V}(t+\tau, x))} \Psi(t, x) = \varphi_{\mathcal{V}}^{\tau}(\Psi(t, x)) + \mathcal{O}(\tau^3) \quad (16)$$

with $\mathcal{V}(s, x) = \mathcal{V}[\phi(s, x), \mathcal{A}(s, x)]$. Note that $\mathcal{V}(s, x) \in \mathbb{C}^{4 \times 4}$ can be orthogonally diagonalized with real eigenvalues (for details, see [3, Appendix 3] and also [19, Chapter 5.2.1]) which allows us to efficiently compute the flow $\Phi_{\mathcal{V}}^{\tau}$.

Following the strategy from [22, Section 4.1] and exploiting the standard bilinear Sobolev estimate $\|uv\|_r \leq K(r, d) \|u\|_r \|v\|_r$ for $r > d/2$ with a constant $K(r, d)$ depending only on r and d (see [1, Theorem 4.39], [15, Theorem 8.3.1] and also [19, Lemma

A.8]), allows us to derive the stability bounds for $\varphi_{\mathcal{N}}^\tau$ and $\Phi_{\mathcal{V}}^\tau$ in H^r with $r > d/2$. For the flow $\varphi_{\mathcal{N}}^\tau$, we obtain

$$\left\| \varphi_{\mathcal{N}}^\tau(\Psi^0) - \varphi_{\mathcal{N}}^\tau(\tilde{\Psi}^0) \right\|_r \leq e^{M_{\mathcal{N}}\tau} \left\| \Psi^0 - \tilde{\Psi}^0 \right\|_r,$$

where $M_{\mathcal{N}}$ depends on $\left\| \Psi^0 \right\|_r$ and $\left\| \tilde{\Psi}^0 \right\|_r$. A similar bound can be shown for $\Phi_{\mathcal{V}}^\tau$, i.e.,

$$\left\| \Phi_{\mathcal{V}}^\tau(\Psi^0) - \Phi_{\mathcal{V}}^\tau(\tilde{\Psi}^0) \right\|_r \leq e^{M_{\mathcal{V}}\tau} \left\| \Psi^0 - \tilde{\Psi}^0 \right\|_r,$$

where $M_{\mathcal{V}}$ depends on $\sup_{t \in [0, T]} (\|\phi(t)\|_r + \|\mathcal{A}(t)\|_r)$.

3.2. Commutator bounds

In order to analyze the local error of our three-term ETSFP scheme (11), we firstly set up commutator bounds for the double commutators involving \mathcal{H} , \mathcal{V} , \mathcal{N} . The commutator $[T, S](v)w$ for (nonlinear) operators T , S is defined via (cf. [22])

$$[T, S](v)w := T'(v)S(v)w - S'(v)T(v)w$$

with $T'(v)$, $S'(v)$ denoting the Fréchet derivative of T and S , respectively.

For sake of compact notation, we define

$$(\boldsymbol{\alpha} \cdot \nabla)\Psi := \sum_{j=1}^d \alpha_j \partial_j \Psi \quad \text{and} \quad (\boldsymbol{\alpha} \cdot \mathcal{A})\Psi := \sum_{j=1}^d \alpha_j A_j \Psi,$$

respectively. The single commutator involving \mathcal{H} and \mathcal{V} applied to Ψ reads

$$\begin{aligned} [\mathcal{H}, \mathcal{V}]\Psi &= -ic \left((\boldsymbol{\alpha} \cdot \nabla \phi)\Psi - (\boldsymbol{\alpha} \cdot \nabla)((\boldsymbol{\alpha} \cdot \mathcal{A})\Psi) + (\boldsymbol{\alpha} \cdot \mathcal{A})(\boldsymbol{\alpha} \cdot \nabla)\Psi \right) \\ &\quad - c^2 [\boldsymbol{\beta}, (\boldsymbol{\alpha} \cdot \mathcal{A})]\Psi. \end{aligned}$$

A short calculation shows that we find the following bound on the corresponding double commutator in H^r , $r > \frac{d}{2}$, i.e.,

$$\|[\mathcal{H}, [\mathcal{H}, \mathcal{V}]](\Psi)\Psi\|_r \leq c^4 K_{\mathcal{A}}^{0,0} + c^3 \left(K_{\mathcal{A}}^{1,1} + K_{\phi}^{1,0} \right) + c^2 \left(K_{\mathcal{A}}^{2,2} + K_{\phi}^{2,2} \right), \quad (17)$$

where the constants $K_{\mathcal{A}}^{j,k}$ and $K_{\phi}^{\ell,m}$ depend on

$$\|\Psi(t)\|_{r+j}, \quad \|\mathcal{A}(t)\|_{r+k} \quad \text{and} \quad \|\Psi(t)\|_{r+\ell} \quad \|\phi(t)\|_{r+m},$$

respectively. In particular, observe that in (17), for vanishing magnetic potential, i.e. $\mathcal{A} \equiv 0$, we have that $K_{\mathcal{A}}^{0,0} = 0$, $K_{\mathcal{A}}^{1,1} = 0$, $K_{\mathcal{A}}^{2,2} = 0$.

Similarly, we establish the following bound on the double commutator involving \mathcal{H} and \mathcal{N} in H^r , $r > d/2$, with a constant where $K_{\mathcal{N}}^2$ depending on $\|\Psi(t)\|_{r+2}$, i.e.,

$$\|[-i\mathcal{H}, [-i\mathcal{H}, \mathcal{N}]](\Psi)\Psi\|_r \leq c^3 \lambda K_{\mathcal{N}}^2.$$

For the remaining double commutators

$$\begin{aligned} & [\mathcal{V}, [\mathcal{V}, \mathcal{H}]], \quad [\mathcal{V}, [\mathcal{V}, \mathcal{N}]], \quad [\mathcal{N}, [\mathcal{N}, \mathcal{V}]], \quad [\mathcal{N}, [\mathcal{N}, -i\mathcal{H}]], \\ & [\mathcal{N}, [\mathcal{N}, \mathcal{V}]], \quad [\mathcal{H}, [\mathcal{V}, \mathcal{N}]], \quad [\mathcal{V}, [\mathcal{H}, \mathcal{N}]], \quad [\mathcal{N}, [\mathcal{H}, \mathcal{V}]] \end{aligned} \quad (18)$$

we establish similar bounds of order $\mathcal{O}(c^2)$ in H^r , $r > \frac{d}{2}$, i.e., replacing X by any of the commutators from (18), we have that $\|X(\Psi)\Psi\|_r \leq c^2 K_X^{1,1,1}$, where the corresponding constants $K_X^{1,1,1}$ depend only on $\|\Psi(t)\|_{r+1}$, $\|\mathcal{A}(t)\|_{r+1}$, $\|\phi(t)\|_{r+1}$. For more information on commutators for nonlinear operators (such as $[\mathcal{H}, [\mathcal{H}, \mathcal{N}]]$), see [22].

4. Error Analysis for the ETSFP scheme

Exploiting the a priori bounds from the previous section we are now ready for a global error analysis of the ETSFP scheme (11) in H^r with $r > d/2$. We carry out the error analysis by a classical Lady-Windermere's fan argument (see [14]) and obtain a second order global error bound $\tau^2(c^4 K_{\mathcal{A}} + c^3 K)$ of the numerical solution, where for $\mathcal{A} \equiv 0$ we have that $K_{\mathcal{A}} = 0$ (see Theorem 1).

4.1. Local error of the ETSFP scheme

In order to derive a local error bound for the scheme (11) combined with the numerical flow approximation (16) to $\varphi_{\mathcal{V}}^\tau$, i.e.,

$$\Psi^{n+1} = \Phi_{ETSFP}^\tau(\Psi^n) = \varphi_{\mathcal{H}}^{\tau/2} \circ \varphi_{\mathcal{N}}^{\tau/2} \circ \Phi_{\mathcal{V}}^\tau \circ \varphi_{\mathcal{N}}^{\tau/2} \circ \varphi_{\mathcal{H}}^{\tau/2}(\Psi^n) \approx \Psi(t_{n+1}), \quad (19)$$

with $\Psi^0 = \Psi(0)$, the idea is to interpret this scheme as a perturbation of the two-term Strang splitting scheme (8) of the nonlinear Dirac equation (4). More precisely, we split the full local error as

$$\begin{aligned} & \left\| \Psi(\tau) - \Phi_{ETSFP}^\tau(\Psi^0) \right\|_r \\ & \leq \left\| \varphi_{\mathcal{H}+\mathcal{V}+\mathcal{N}}^\tau(\Psi^0) - \varphi_{\mathcal{H}}^{\tau/2} \circ \varphi_{\mathcal{V}+\mathcal{N}}^\tau \circ \varphi_{\mathcal{H}}^{\tau/2}(\Psi^0) \right\|_r \\ & \quad + \left\| \varphi_{\mathcal{H}}^{\tau/2} \circ \varphi_{\mathcal{V}+\mathcal{N}}^\tau \circ \varphi_{\mathcal{H}}^{\tau/2}(\Psi^0) - \Phi_{ETSFP}^\tau(\Psi^0) \right\|_r, \end{aligned} \quad (20)$$

where we denote $\varphi_{\mathcal{H}+\mathcal{V}+\mathcal{N}}^\tau(\Psi^0) = \Psi(\tau)$ the exact flow of the full system. We observe that the first difference term is just the local error of the two term Strang splitting (8). Thus, a classical analysis as in [12, 22] shows that

$$\begin{aligned} & \left\| \varphi_{\mathcal{H}+\mathcal{V}+\mathcal{N}}^\tau(\Psi^0) - \varphi_{\mathcal{H}}^{\tau/2} \circ \varphi_{\mathcal{V}+\mathcal{N}}^\tau \circ \varphi_{\mathcal{H}}^{\tau/2}(\Psi^0) \right\|_r \\ & \leq \tau^3 K \cdot \left(c^4 K_{\mathcal{A}}^{0,0} + c^3 \left(K_{\mathcal{A}}^{1,1} + K_{\phi}^{1,0} \right) + c^2 \left(K_{\mathcal{A}}^{2,2} + K_{\phi}^{2,2} \right) \right), \end{aligned} \quad (21)$$

where the constants $K_{\mathcal{A}}^{j,k}$, $K_{\phi}^{\ell,m}$, arising from the commutator bounds in Section 3.2, are given in (17) and where the constant K is independent of c and τ . In particular note, that for $\mathcal{A} \equiv 0$ all constants $K_{\mathcal{A}}^{j,k} = 0$ vanish.

In order to derive a bound for the second term in (20), we exploit that by (13) $\varphi_{\mathcal{H}}^\tau$ is a linear isometry in H^r . Thus, that term can be bounded by

$$\left\| \varphi_{\mathcal{V}+\mathcal{N}}^\tau \left(\varphi_{\mathcal{H}}^{\tau/2}(\Psi^0) \right) - \left(\varphi_{\mathcal{N}}^{\tau/2} \circ \Phi_{\mathcal{V}}^\tau \circ \varphi_{\mathcal{N}}^{\tau/2} \right) \left(\varphi_{\mathcal{H}}^{\tau/2}(\Psi^0) \right) \right\|_r \leq \tau^3 K_{\mathcal{V},\mathcal{N}}, \quad (22)$$

i.e., we can interpret it as a second order perturbation term for the two-term splitting. The constant $K_{\mathcal{V},\mathcal{N}}$ depends on the double commutator bounds of \mathcal{V} and \mathcal{N} from Section 3.2, which involve $\|\Psi(t)\|_r$, $\|\mathcal{A}(t)\|_r$, $\|\phi(t)\|_r$, but which are independent of c . Combining the local error bounds (21) and (22) yields for the full local error (20)

$$\begin{aligned} & \left\| \Psi(\tau) - \Phi_{ETSFP}^\tau(\Psi^0) \right\|_r \\ & \leq \tau^3 K \cdot \left(c^4 K_{\mathcal{A}}^{0,0} + c^3 \left(K_{\mathcal{A}}^{1,1} + K_\phi^{1,0} \right) + c^2 \left(K_{\mathcal{A}}^{2,2} + K_\phi^{2,2} \right) + K_{\mathcal{V},\mathcal{N}} \right), \end{aligned}$$

where the constants $K_{\mathcal{A}}^{j,k}$ and $K_\phi^{\ell,m}$ and $K_{\mathcal{V},\mathcal{N}}$ are given in (21) and (22) and where K is independent of c and τ .

4.2. Global Error bound

In order to obtain a global error bound for the ETSFP time integration scheme (19), we combine the local error bound of the previous section with the stability bounds from Section 3.1. By a classical Lady Windermere's fan argument (see [14]), we thus obtain the following bound on the global error, i.e.,

$$\begin{aligned} & \left\| \Psi(t_n) - \left(\Phi_{ETSFP}^\tau \right)^n (\Psi^0) \right\|_r \\ & \leq \tau^2 e^{T\mathcal{M}} K \cdot \left(c^4 K_{\mathcal{A}}^{0,0} + c^3 \left(K_{\mathcal{A}}^{1,1} + K_\phi^{1,0} \right) + c^2 \left(K_{\mathcal{A}}^{2,2} + K_\phi^{2,2} \right) + K_{\mathcal{V},\mathcal{N}} \right), \end{aligned} \quad (23)$$

where the constant \mathcal{M} depends on the H^r norms of the potentials $\mathcal{A}(t)$ and $\phi(t)$ and on the initial data Ψ^0 and where the constants $K_{\mathcal{A}}^{j,k}$ and $K_\phi^{\ell,m}$ and $K_{\mathcal{V},\mathcal{N}}$ are given in (21) and (22) and where K is independent of c and τ .

4.3. Error of the full discretization

We obtain a fully discrete Splitting scheme for approximating the solution of (1) by combining the scheme Φ_{ETSFP}^τ from (19) with a Fourier Pseudospectral space discretization scheme, which discretizes the spatial operator $\mathcal{H}\Psi$ from (1) and (3), respectively. In the following, we denote by Φ_{ETSFP}^{τ, M_x} the full discretization of the scheme Φ_{ETSFP}^τ with $M_x \in \mathbb{N}$ spatial grid points in each spatial direction. For an extensive overview over Fourier Pseudospectral space discretization techniques, see for example [12, 21].

The error of the fully discrete scheme Φ_{ETSFP}^{τ, M_x} measured in a discrete H^r norm for $r > d/2$ then satisfies

$$\begin{aligned} & \left\| \Psi(t_n) - \left(\Phi_{ETSFP}^{\tau, M_x} \right)^n (\Psi^0) \right\|_r \\ & \leq \tau^2 e^{T\mathcal{M}} K \cdot \left(c^4 K_{\mathcal{A}}^{0,0} + c^3 \left(K_{\mathcal{A}}^{1,1} + K_\phi^{1,0} \right) + c^2 \left(K_{\mathcal{A}}^{2,2} + K_\phi^{2,2} \right) + K_{\mathcal{V},\mathcal{N}} \right) \\ & \quad + M_x^{-(m-r)}, \end{aligned}$$

where m explicitly depends on the regularity of Ψ , ϕ , \mathcal{A} , and where the constants \mathcal{M} , $K_{\mathcal{A}}^{j,k}$ and $K_{\phi}^{\ell,m}$ and $K_{\mathcal{V},\mathcal{N}}$ are given in (23), (21) and (22) and where K is independent of c and τ .

We summarize the convergence results in more detail in the following [Theorem 1](#).

Theorem 1. *Fix $c \geq 1$, $\lambda \in \mathbb{R}$, r_1 , $r > d/2$ and $\epsilon > 0$ arbitrarily small. Furthermore, let $r'_1 = \max\{2, r_1 + d/2 + \epsilon\}$. Let the initial data of the Dirac equation (1) with $\lambda \in \mathbb{R}$ satisfy $\Psi^0 \in H^{r+r'_1}$ and let Ψ be the solution to the Dirac equation (1).*

Then there exist constants $T, \tau_0 > 0$ such that for $\tau \leq \tau_0$ and $M_x \geq M_0$ grid points in space, and with the choice of potentials $\mathcal{A}(t, \cdot)$, $\phi(t, \cdot) \in H^{r+r'_1}$, we obtain

$$\begin{aligned} & \|\Psi(t_n) - \Psi_{M_x}^n\|_r \\ & \leq \tau^2 e^{T\mathcal{M}} K \cdot \left(c^4 K_{\mathcal{A}}^{0,0} + c^3 \left(K_{\mathcal{A}}^{1,1} + K_{\phi}^{1,0} \right) + c^2 \left(K_{\mathcal{A}}^{2,2} + K_{\phi}^{2,1} \right) + K_{\mathcal{V},\mathcal{N}} \right) \\ & \quad + M_x^{-r_1}, \end{aligned}$$

where $\Psi_{M_x}^n = \left(\Phi_{ETSGFP}^{\tau, M_x} \right)^n (\Psi_{M_x}^0)$ and where the constants \mathcal{M} , K , $K_{\mathcal{A}}^{j,k}$, $K_{\phi}^{\ell,m}$ and $K_{\mathcal{V},\mathcal{N}}$ are given in (23), (21) and (22), respectively. In particular note that for $\mathcal{A} \equiv 0$, we have that $K_{\mathcal{A}}^{j,j} = 0$, $j = 0, 1, 2$, i.e., the error constant depends only on c^3 and not on c^4 .

Proof. Applying the line of argumentation from [4] and [22] and exploiting the results from the previous sections yields the desired convergence bound. \square

Our numerical results in [Section 6](#) below underline the second order convergence in time for time steps $\tau \lesssim c^{-2}$. They furthermore suggest that the error bounds from the previous [Theorem 1](#) can be refined to the order $\mathcal{O}(\tau^2 c^2)$ similar to [4, Theorem 4.4] under particular (technical) assumptions on the time steps τ , i.e., from our numerical results we observe

$$\|\Psi(t_n) - \Psi_{M_x}^n\|_r = \mathcal{O}(\tau^2 c^2). \quad (24)$$

A rigorous proof based on the ideas from [4, Proof of Theorem 4.4] of this improved bound may be interesting future research.

5. Nonlinear Dirac Equations in the Nonrelativistic Limit Regime

It is well-know, that in the non-relativistic limit regime, i.e., for $c \rightarrow \infty$, the class of Dirac and Klein–Gordon type equations with highly-oscillatory solution asymptotically reduce to a system of c -independent (nonlinear) Schrödinger equations with (non-oscillatory) solution $(u_{\infty}, v_{\infty})^{\top}$ (see for example [26], and also [13, 18, 19, 23, 24] for the case of cubic Klein–Gordon equations and Maxwell–Klein–Gordon and Maxwell–Dirac systems). Thereby the highly oscillatory nature of the exact solution is contained only in a multiplicative highly-oscillatory phase $e^{ic^2 t}$. More precisely we have that for $c \rightarrow \infty$,

$$\Psi(t) = \Psi_{\infty}(t) + \mathcal{O}(c^{-1}), \quad \Psi_{\infty}(t) = \frac{1}{2} \left(e^{ic^2 t} u_{\infty}(t) + e^{-ic^2 t} v_{\infty}(t) \right). \quad (25)$$

To see this structure, we firstly rewrite (1) as an equivalent nonlinear Klein–Gordon (KG) system for the components ψ_j , $j = 1, 2, 3, 4$ of Ψ and apply a suitable variable transform $(\Psi, \partial_t \Psi) \mapsto (u, v)$, where u, v both satisfy a first order in time system of equations (see for example [13, 19, 23, 24]). Then, following the strategy from [13, 18, 19, 23, 24], we find the following bounds in the sense of the H^r -norm, $r > d/2$,

$$u(t) = e^{ic^2 t} u_\infty(t) + \mathcal{O}(c^{-1}) \quad \text{and} \quad v(t) = e^{ic^2 t} v_\infty(t) + \mathcal{O}(c^{-1}),$$

where $(u_\infty, v_\infty)^\top$ solves the nonlinear Schrödinger system

$$\begin{aligned} i\partial_t u_\infty &= \frac{1}{2}\Delta u_\infty + \phi(t)u_\infty + \frac{1}{4}\lambda(|u_\infty|^2 - |v_\infty|^2)u_\infty \\ i\partial_t v_\infty &= \frac{1}{2}\Delta v_\infty - \phi(t)v_\infty + \frac{1}{4}\lambda(|u_\infty|^2 - |v_\infty|^2)v_\infty, \\ u_\infty(0) &= (0, 0, 2\psi_3(0), 2\psi_4(0))^\top, \quad v_\infty(0) = (2\overline{\psi_1(0)}, 2\overline{\psi_2(0)}, 0, 0)^\top. \end{aligned} \quad (26)$$

Therefore,

$$\|\Psi(t) - \Psi_\infty(t)\|_r \leq Kc^{-1}, \quad (27)$$

where K depends on $\|\Psi(0)\|_{r+4}$ and $\|\phi(t)\|_{r+4}$, i.e., we require

$$\Psi(0) \in H^{r+4} \quad \text{and} \quad \phi(t) \in H^{r+4} \quad \text{for all } t \in [0, T]. \quad (28)$$

This result is underlined by numerical experiments below, where we apply a three-term Strang splitting to (26) with step size τ . The resulting numerical limit approximation Ψ_∞^n from (25) towards the exact solution $\Psi(t_n)$ then satisfies error bounds of order $\mathcal{O}(\tau^2 + c^{-1})$ (cf. [13, 16, 19] for the case of other Klein–Gordon and Dirac type systems). In particular, the experiments suggest that the regularity assumptions (28) on the exact solution are sharp, i.e., the bound (27) does not hold, if the regularity assumptions are violated.

6. Numerical Experiments

In this section, we numerically underline the theoretical results from Theorem 1. Note that in lower dimensions $d = 1, 2$ the nonlinear Dirac system (1) with four-component solution $\Psi(t, x) \in \mathbb{C}^4$ reduces to a system for a two-component solution $\tilde{\Psi}(t, x) \in \mathbb{C}^2$ (see for example [3, 4, 19, 26]). For sake of simplicity, we thus consider in this section the following reduced equation for $d = 2$,

$$i\partial_t \tilde{\Psi} = -ic \sum_{j=1}^d \sigma_j \partial_j \tilde{\Psi} + c^2 \sigma_3 \tilde{\Psi} + \left(\phi - \sum_{j=1}^d \sigma_j A_j \right) \tilde{\Psi} + \lambda(\tilde{\Psi} \cdot \sigma_3 \bar{\tilde{\Psi}}) \sigma_3 \tilde{\Psi} \quad (29)$$

with initial data $\tilde{\Psi}(0, x) = \Psi^0(x) \in \mathbb{C}^2$ and for $c \geq 1$, $\lambda \geq 0$. The construction of the respective splitting scheme and the theoretical results from the previous sections also apply to the latter reduced system. In the following, we omit the $\tilde{\cdot}$ for simplicity.

In particular, in view of the asymptotic convergence of the exact solution Ψ towards the limit approximation Ψ_∞ , our numerical experiments shall stress the importance of the spatial regularity assumptions on the initial data and the potentials. We thus construct data of a certain regularity as described in the following section.

6.1. Construction of data of a certain regularity

In order to construct a function $u \in H^r(\mathbb{T}^d)$, $r \geq 0$, we proceed as follows. Let u_R with $u_R(x) \in [-1, 1]$ for all $x \in \mathbb{T}^d$ be a random distribution of data values in \mathbb{T}^d . Then the function defined via

$$u(x) = \sum_{k \in \mathbb{Z}^d} (1 + |k|)^{-(r+d/2)} (\widehat{u_R})_k e^{ikx} \quad \text{for all } x \in \mathbb{T}^d$$

has bounded H^r norm, but unbounded $H^{r+\epsilon}$, $\epsilon > 0$ norm.

In practical implementation for the case of $d = 2$, we obtain a discrete version of such a function via (`fft2` and `ifft2` are the MATLAB inverse fast Fourier routines)

$$U = \text{Reg}(U_R, r) := \text{ifft2} \left((1 + |k|)^{-(r+d/2)} \text{fft2}(U_R) \right), \quad k \in \mathcal{Z}_{M_x}^d, \quad (30)$$

where $U_R \in [-1, 1]^{M_x \times M_x}$ denotes randomly distributed values on a 2-dimensional tensor grid with $M_x \in \mathbb{N}$ equidistant points in each spatial direction, and where

$$\mathcal{Z}_{M_x} := \begin{cases} \{-R, \dots, R-1\}, & \text{if } M_x = 2R \in \mathbb{N} \text{ is even,} \\ \{-R, \dots, R\}, & \text{if } M_x = 2R + 1 \in \mathbb{N} \text{ is odd} \end{cases}$$

is a finite index set.

6.2. Numerical Experiments

For practical implementation issues, we focus on a 2D spatial grid, i.e., we choose

$$d = 2 \quad \text{and} \quad M_x = 128 \quad \text{grid points in each direction.}$$

Moreover, fix $T = 1$ and choose parameter values $c = c_j \in [1, 2000]$, $j = 1, \dots, 90$ with

$$c_j = \exp((j-1) \log(2000)/89)$$

where $\log(c_j)$ is distributed equidistantly in the interval $[0, \log(2000)]$.

For given time step size τ , we apply our fully discrete scheme (see [Section 4.3](#))

$$\Phi_{ETSFPP}^{\tau, M_x}(\Psi_{M_x}^0) := \left(\varphi_{\mathcal{H}}^{\frac{\tau}{2}, M_x} \circ \varphi_{\mathcal{N}}^{\frac{\tau}{2}, M_x} \circ \Phi_{\mathcal{V}}^{\tau, M_x} \circ \varphi_{\mathcal{N}}^{\frac{\tau}{2}, M_x} \circ \varphi_{\mathcal{H}}^{\frac{\tau}{2}, M_x} \right) (\Psi_{M_x}^0) \quad (31)$$

to the reduced system (29), where the index M_x denotes the spatial discretization with M_x grid points in each direction, and where $\Phi_{\mathcal{V}}^{\tau, M_x}$ denotes the exponential trapezoidal rule approximation to the exact flow $\varphi_{\mathcal{V}}^{\tau}$, see (16). In our simulations, for fixed number $N_{\max} = 5040$ with m_{\max} divisors, we choose time step sizes

$$\tau_m = T/N_m, \quad m = 1, \dots, m_{\max}.$$

Moreover, let $\tau_{\min} = \min_m \tau_m$ be the smallest of the chosen time step sizes.

6.2.1. Reference Solution

We compute a reference approximation Ψ_{ref}^n to the exact solution $\Psi(t_n)$ of the non-linear Dirac equation (29) at time $t_n = n\tau_{\text{min}}$, $n = 0, 1, 2, \dots, \lfloor T/\tau_{\text{min}} \rfloor$ with the following scheme with a very small time step size $\tau_{\text{ref}} = \tau_{\text{min}}/M_{\text{ref}}$, $M_{\text{ref}} = 256$, i.e., $\tau_{\text{ref}} = (N_{\text{max}} \cdot M_{\text{ref}})^{-1} \approx 7.8 \cdot 10^{-7}$ and

$$\Phi_{\text{ref}}^{\tau_{\text{min}}, M_x}(\Psi_{M_x}^0) := \left(\varphi_{\mathcal{H}}^{\frac{\tau_{\text{ref}}}{2}, M_x} \circ \Phi_{\text{Heun}}^{\tau_{\text{ref}}, M_x} \circ \varphi_{\mathcal{H}}^{\frac{\tau_{\text{ref}}}{2}, M_x} \right)^{M_{\text{ref}}} (\Psi_{M_x}^0).$$

Thereby, we apply the second order in time method of Heun $\Phi_{\text{Heun}}^{\tau, M_x}$ to subproblem (7), in order to approximate the corresponding exact flow $\varphi_{\mathcal{V}+\mathcal{N}}^{\tau}$ in the splitting scheme (6). More precisely, we have that at time t_n

$$\begin{aligned} \Phi_{\text{Heun}}^{\tau, M_x}(Z_{M_x}^n) &= Z_{M_x}^n + \frac{\tau}{2} \left(-i\mathcal{V}(t_n)Z_{M_x}^n - i\mathcal{N}(Z_{M_x}^n) \right. \\ &\quad \left. - i\mathcal{V}(t_{n+1})\widetilde{Z}_{M_x}^{n+1} - i\mathcal{N}(\widetilde{Z}_{M_x}^{n+1}) \right), \quad \text{where} \\ \widetilde{Z}_{M_x}^{n+1} &= Z_{M_x}^n + \tau \left(-i\mathcal{V}(t_n)Z_{M_x}^n - i\mathcal{N}(Z_{M_x}^n) \right). \end{aligned}$$

6.2.2. Numerical Results

In order to have comparable data in all our numerical simulations of the solution $\Psi_{M_x}(t)$ of the spatially discretized system (29) in $d = 2$ spatial dimensions, we firstly define in MATLAB random data arrays (in exactly that order) $\psi_{1,R}^0, \psi_{2,R}^0$ using the MATLAB function `rand(M_x)-rand(M_x)+1i` (`rand(M_x)-rand(M_x)`), and $\phi_R, A_{1,R}, A_{2,R}$ using the MATLAB function `rand(M_x)-rand(M_x)`, where we control the random number generator with the MATLAB command `rng(1)` (i.e., we choose seed '1'). We then choose constants $r_{\Psi}, r_{\phi}, r_{\mathcal{A}}$ (see specifications in the experiment description below) and construct corresponding functions $\widetilde{\psi}_1^0, \widetilde{\psi}_2^0 \in H^{r_{\Psi}}, \widetilde{\phi} \in H^{r_{\phi}}, \widetilde{A}_1, \widetilde{A}_2 \in H^{r_{\mathcal{A}}}$, of bounded discrete H^{r_X} ($X \in \{\Psi, \phi, \mathcal{A}\}$) norm by applying `Reg(\cdot, r_X)`, $X \in \{\Psi, \phi, \mathcal{A}\}$ from (30) to the respective random arrays $\psi_{1,R}^0, \psi_{2,R}^0$ and $\phi_R, A_{1,R}, A_{2,R}$. In the experiments below, we then consider system (29) with the following L^2 -normalized initial data

$$\Psi_{M_x}^0 = \begin{pmatrix} \psi_1^0 \\ \psi_2^0 \end{pmatrix} := \left(\left\| \widetilde{\psi}_1^0 \right\|_{L^2}^2 + \left\| \widetilde{\psi}_2^0 \right\|_{L^2}^2 \right)^{-\frac{1}{2}} \begin{pmatrix} \widetilde{\psi}_1^0 \\ \widetilde{\psi}_2^0 \end{pmatrix} \quad (32)$$

and time-dependent potentials

$$\begin{aligned} \phi_{M_x}(t) &:= \cos(4t) \left\| \widetilde{\phi} \right\|_{L^2}^{-1} \widetilde{\phi}, \\ \mathcal{A}_{M_x}(t) &= \begin{pmatrix} A_1(t) \\ A_2(t) \end{pmatrix} := \left(\left\| \widetilde{A}_1 \right\|_{L^2}^2 + \left\| \widetilde{A}_2 \right\|_{L^2}^2 \right)^{-\frac{1}{2}} \begin{pmatrix} \cos(2t)\widetilde{A}_1 \\ \sin(3t)\widetilde{A}_2 \end{pmatrix}. \end{aligned} \quad (33)$$

In the following, we fix $r = 1.1 > d/2$ and discuss numerical simulation results for initial data (32) of regularity r_{Ψ} and potentials (33) of regularity $r_{\phi}, r_{\mathcal{A}}$. We illustrate the smoothness of the constructed data in Fig. 1, where we plotted the real part of the random data $\psi_{1,R}^0$ and its regularized and normalized correspondence $\text{Re}(\psi_1^0)$ for different regularity. Next, we discuss various experiments, where the corresponding Figures show

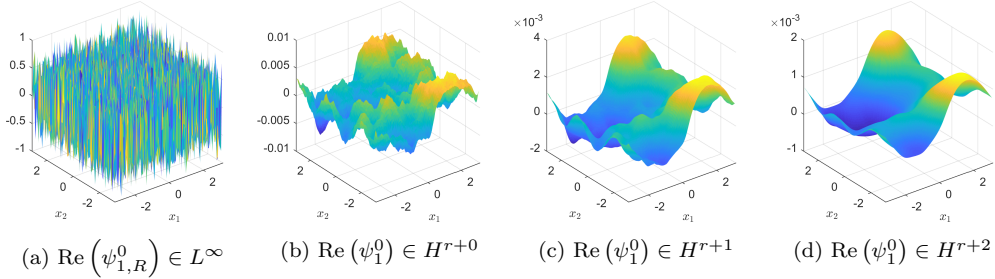


Figure 1: Data of different regularity for $r = 1.1$, regularized from the random distribution $\psi_{1,R}^0$ (left).

the numerical errors

$$\max_{t_n \in [0, T]} \left\| \Psi_{\text{ref}}^{M_x}(t_n) - \Psi_{M_x}^n \right\|_r$$

of the ETSFP approximation obtained with the scheme (31) and analogously the errors of the numerical limit approximation Ψ_{∞, M_x}^n (cf. (25)). Note, that the coloured thick and thin lines in the left and middle plot correspond to pairs (τ, c) with $\tau \lesssim c^{-2}$ and $\tau \gtrsim c^{-2}$, respectively. We start off with experiments for the general case of the reduced system (29).

Experiment 1. Fix $\lambda = 2$ and choose $r_{\Psi} = r_{\phi} = r_{\mathcal{A}} = r + 2$. The numerical results in Fig. 2 underline the improved convergence bound $\mathcal{O}(\tau^2 c^2)$ of the ETSFP scheme for $\tau \sim c^{-2}$ (cf. (24)) for the regularity assumptions from Theorem 1 and (24). Moreover, we observe that the error of limit approximation (25) towards the reference solution shows a weaker convergence than $\mathcal{O}(c^{-1})$ which is due to lower regularity of the data than needed for this bound (cf. (28)).

Experiment 2 (data of higher regularity). Fix $\lambda = 2$ and choose $r_{\Psi} = r_{\phi} = r + 4$, $r_{\mathcal{A}} = r + 2$. From Fig. 3, we observe slightly better error constants for the ETSFP scheme compared to Experiment 1. On the other hand for the limit approximation (25) we observe the expected $\mathcal{O}(c^{-1})$ convergence in contrast to Experiment 1 which underlines the importance of the data regularity for this approximation (cf. (28)).

Experiment 3 (data of lower regularity). Fix $\lambda = 2$ and choose $r_{\Psi} = r_{\phi} = r_{\mathcal{A}} = r$. From Fig. 4, we observe a severe order reduction for our ETSFP scheme for large time steps τ if we choose data of lower regularity. The convergence of order 2 can be observed only for very small time steps τ . Moreover, under these low regularity conditions the limit approximation (25) shows a very bad convergence behaviour, which underlines once more the necessity of the regularity assumptions (28).

In the following experiments, we consider (29) with vanishing vector potential, i.e., $\mathcal{A} \equiv 0$. We observe a significantly better convergence behaviour of the ETSFP scheme than for $\mathcal{A} \neq 0$.

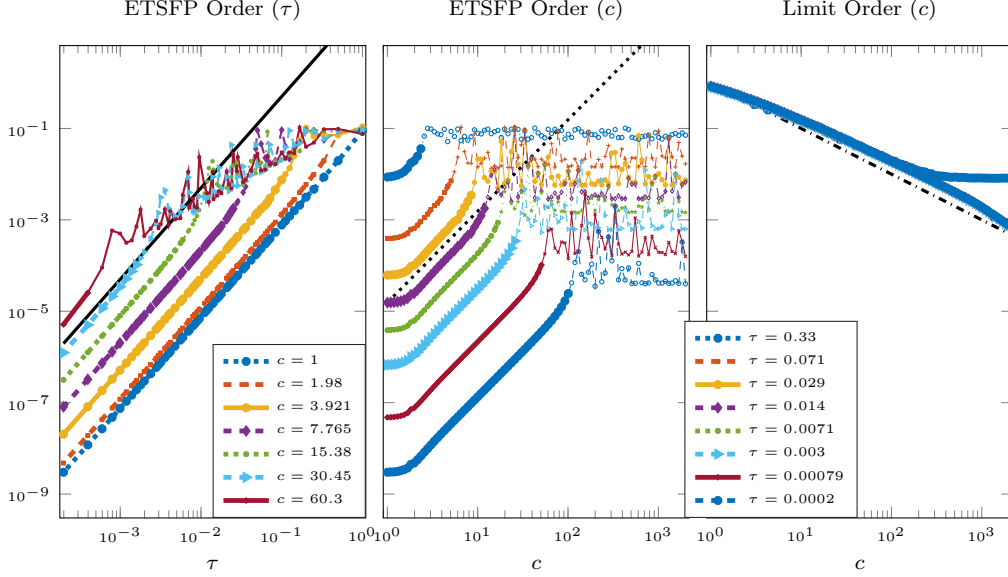


Figure 2: Plots for [Experiment 1](#): *Left and middle*: Convergence order of the ETSFP scheme in τ and c . The black solid and dotted lines correspond to order τ^2 and c^2 , respectively. *Right*: Convergence of the limit approximation (25) in c . The black dotted line corresponds to the order c^{-1} .

Experiment 4. Fix $\mathcal{A} \equiv 0$, $\lambda = 2$ and choose $r_\Psi = r_\phi = r + 2$. [Fig. 5](#) illustrates that for vanishing vector potential, i.e., $\mathcal{A} \equiv 0$, we observe significantly better errors for the ETSFP scheme than for the general case in the previous experiments. This underlines, that the main contribution in the error bounds for the ETSFP scheme for the general case is given through the terms involving the vector potential \mathcal{A} (cf. [Theorem 1](#)). The limit approximation (25) shows the same behaviour as in [Experiment 1](#) since the regularity assumptions from (28) on the data are violated.

Experiment 5 (data of higher regularity). Fix $\mathcal{A} \equiv 0$, $\lambda = 2$ and choose $r_\Psi = r_\phi = r + 4$. Considering data of higher regularity than in [Experiment 4](#), we observe in [Fig. 6](#) that the ETSFP scheme shows a much better error behaviour with respect to c . Moreover, we observe that for $\tau \lesssim c^{-2}$ (thick lines) and for $c > K(\tau)$ for some number $K(\tau)$ depending on τ , the error of the ETSFP scheme is bounded in $\mathcal{O}(\tau^2)$ independent of c . On the other hand for the limit approximation (25), we observe similar to [Experiment 2](#) the expected $\mathcal{O}(c^{-1})$ convergence in contrast to [Experiment 1](#) and [Experiment 4](#) which underlines the importance of the data regularity for this approximation (cf. (28)).

In the following experiments, we consider (29) with vanishing vector potential and for vanishing nonlinearity, i.e., $\mathcal{A} \equiv 0$ and $\lambda = 0$. For data of enough regularity, we observe almost uniform second order convergence in time of the ETSFP scheme, i.e., the error constants do not depend on c .

Experiment 6. Fix $\mathcal{A} \equiv 0$, $\lambda = 0$ and choose $r_\Psi = r_\phi = r + 2$. In [Fig. 7](#), we observe similar to [Experiment 5](#) that for $\tau \lesssim c^{-2}$ (thick lines) and for $c > K(\tau)$ for some number

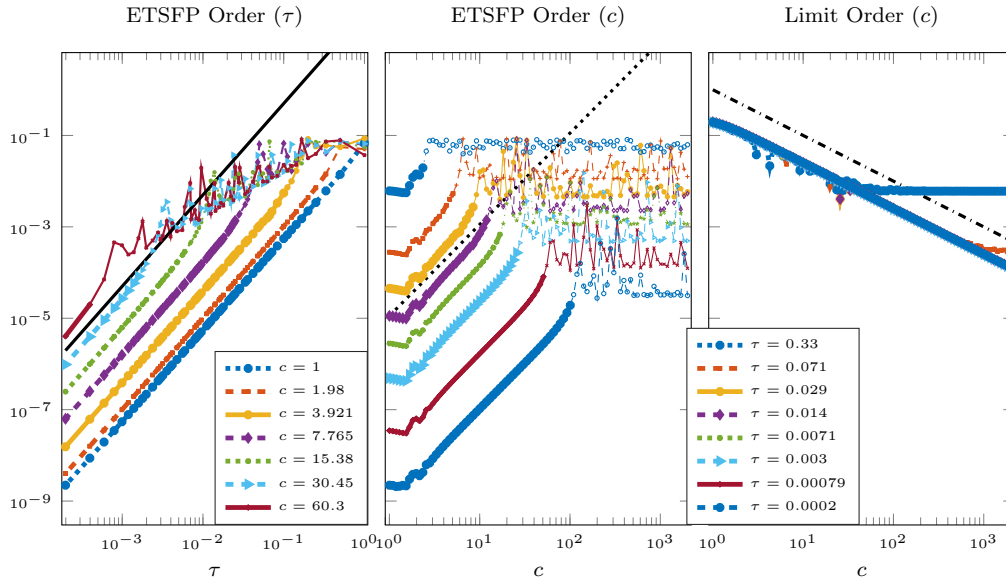


Figure 3: Plots for [Experiment 2](#): *Left and middle*: Convergence order of the ETSFP scheme in τ and c . The black solid and dotted lines correspond to order τ^2 and c^2 , respectively. *Right*: Convergence of the limit approximation (25) in c . The black dotted line corresponds to the order c^{-1} .

$K(\tau)$ depending on τ , the error of the ETSFP scheme is $\mathcal{O}(\tau^2)$ independent of c . The limit approximation (25) shows the same behaviour as in [Experiment 1](#) and [Experiment 4](#) since the regularity assumptions from [Section 5](#) on the data are violated (cf. (28)).

Experiment 7 (data of higher regularity). Fix $\mathcal{A} \equiv 0$, $\lambda = 0$ and choose $r_\Psi = r_\phi = r + 4$. [Fig. 8](#) shows similar to [Experiment 5](#), [Experiment 6](#) that for $\tau \lesssim c^{-2}$ (thick lines) and for $c > K(\tau)$ for some number $K(\tau)$ depending on τ , the error of the ETSFP scheme is $\mathcal{O}(\tau^2)$ independent of c . We observe, that the peaks in the c -convergence plot are smaller than in the previous experiments. For the limit approximation (25), we observe similar $\mathcal{O}(c^{-1})$ convergence results as in [Experiment 2](#) and [Experiment 5](#).

7. Interesting Future Research

In our numerical results for the numerical solution of the Dirac equation (1) with Thirring type interaction, we observed an improved error behaviour of our ETSFP scheme of order $\mathcal{O}(\tau^2 c^2)$ for step sizes $\tau \lesssim c^{-2}$. Thus it would be interesting future research to give a rigorous proof for this bound, which is similar to the bound from [4, Theorem 4.4] for the case of the Dirac equation with Soler interaction.

Moreover, building up on our ETSFP scheme, it would be interesting to construct a splitting scheme for solving a nonlinear Dirac–Poisson equation with Thirring type

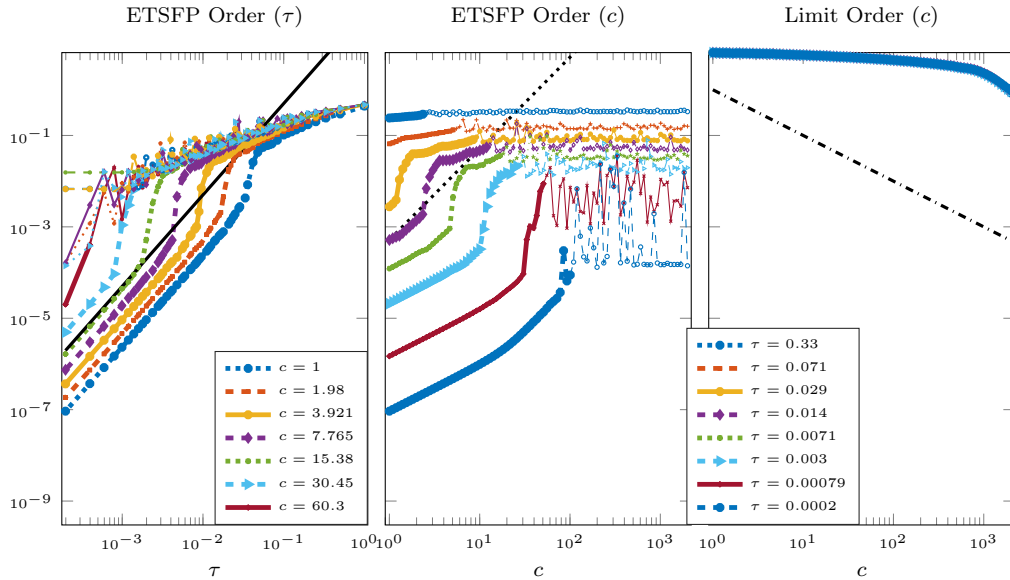


Figure 4: Plots for [Experiment 3](#): *Left and middle*: Convergence order of the ETSFP scheme in τ and c . The black solid and dotted lines correspond to order τ^2 and c^2 , respectively. *Right*: Convergence of the limit approximation (25) in c . The black dotted line corresponds to the order c^{-1} .

interaction, i.e.,

$$\begin{cases} i\partial_t \Psi = \mathcal{H}\Psi + \mathcal{V}[\phi, \mathcal{A}]\Psi + \mathcal{N}(\Psi), & \Psi(0, x) = \Psi^0(x) \in \mathbb{C}^4, \\ -\Delta\phi = |\Psi|^2, \end{cases} \quad (34)$$

where \mathcal{A} is a given vector potential, and where ϕ is given through a Poisson equation with Dirac charge density on the right hand side. In the construction of such a scheme, we suggest to split the problem as in [Section 2.3](#), but replace subproblem (9b) by

$$\begin{cases} i\partial_t \Psi = \mathcal{V}[\phi, \mathcal{A}]\Psi, & \Psi(0, x) = \Psi^0 \in \mathbb{C}^4, \\ -\Delta\phi = |\Psi|^2, \end{cases}$$

which can be solved exactly since $\partial_t |\Psi|^2 = 0$. An error analysis can be carried out using the ideas and techniques given in [\[22\]](#) for the case of the Schrödinger–Poisson equation and [\[4\]](#) for the case of the Soler type nonlinear Dirac equation. Preliminary numerical results are promising.

Acknowledgement

We gratefully acknowledge financial support by the Deutsche Forschungsgemeinschaft (DFG) through CRC 1173.

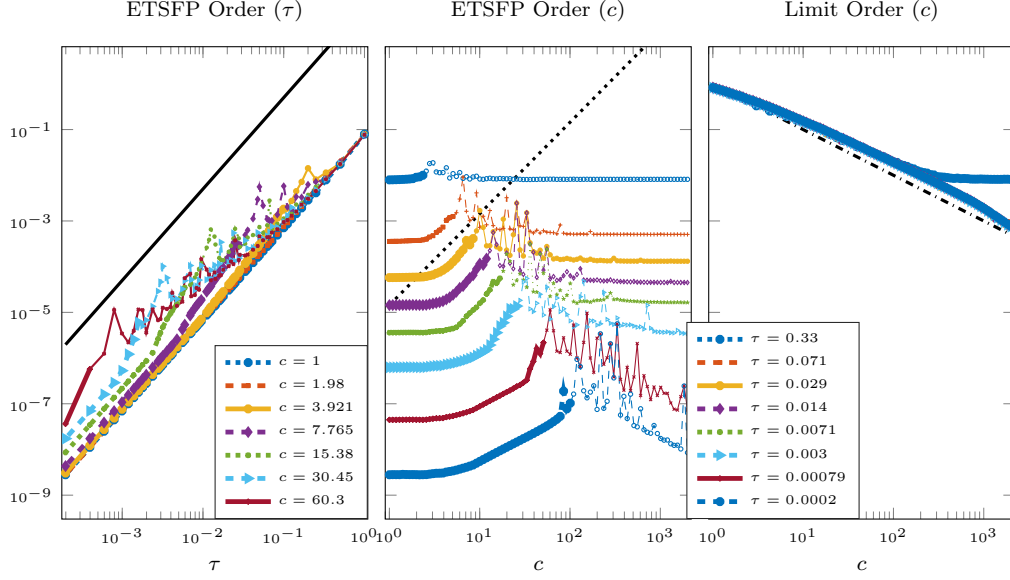


Figure 5: Plots for [Experiment 4](#): *Left and middle*: Convergence order of the ETSFP scheme in τ and c . The black solid and dotted lines correspond to order τ^2 and c^2 , respectively. *Right*: Convergence of the limit approximation (25) in c . The black dotted line corresponds to the order c^{-1} .

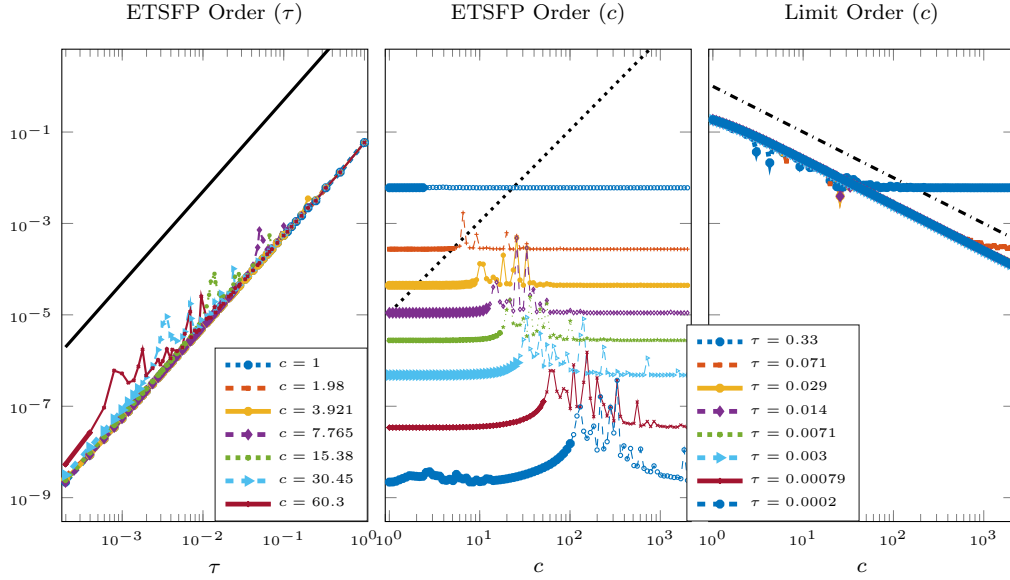


Figure 6: Plots for [Experiment 5](#): *Left and middle*: Convergence order of the ETSFP scheme in τ and c . The black solid and dotted lines correspond to order τ^2 and c^2 , respectively. *Right*: Convergence of the limit approximation (25) in c . The black dotted line corresponds to the order c^{-1} .

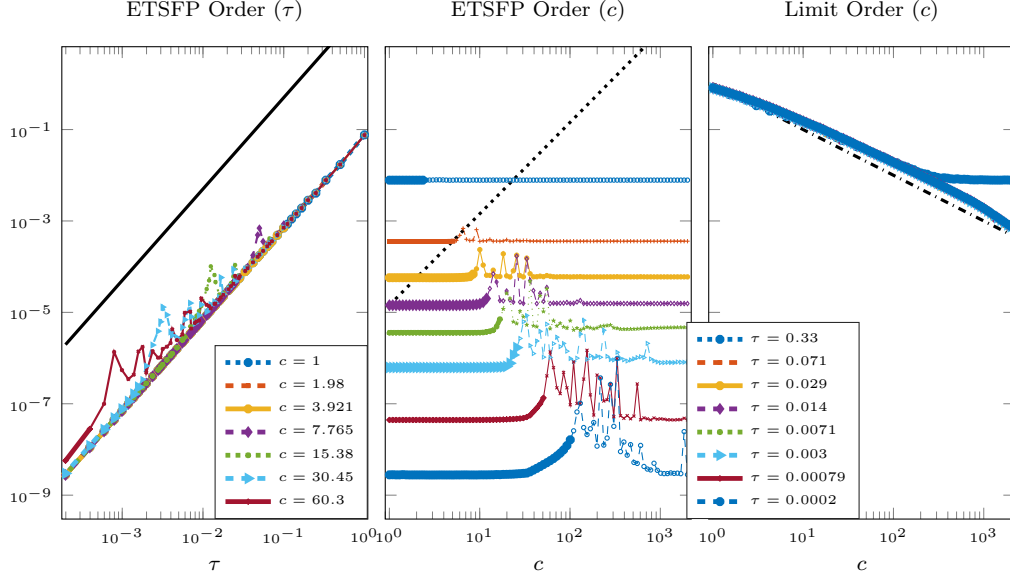


Figure 7: Plots for [Experiment 6](#): *Left and middle*: Convergence order of the ETSFP scheme in τ and c . The black solid and dotted lines correspond to order τ^2 and c^2 , respectively. *Right*: Convergence of the limit approximation (25) in c . The black dotted line corresponds to the order c^{-1} .

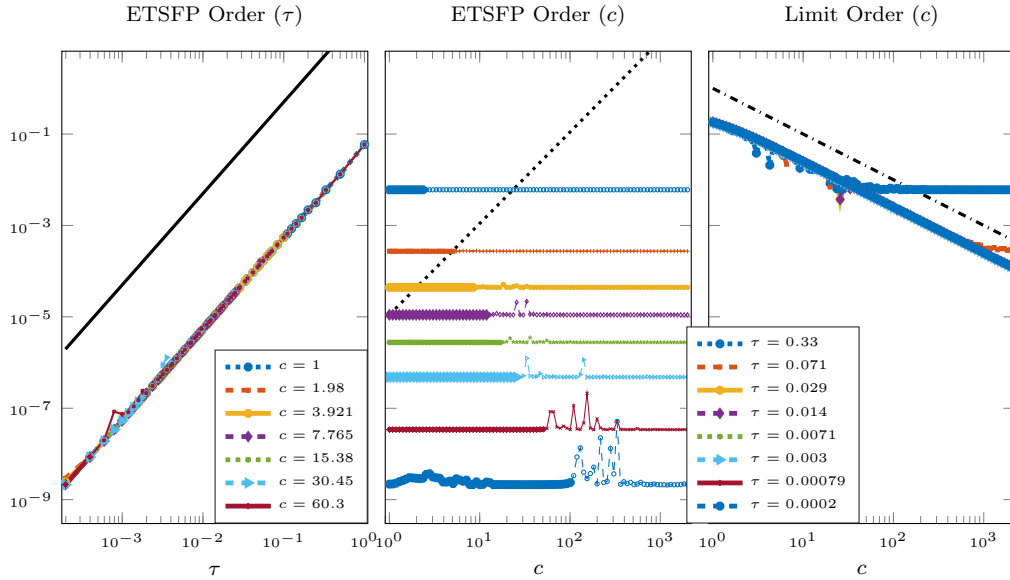


Figure 8: Plots for [Experiment 7](#): *Left and middle*: Convergence order of the ETSFP scheme in τ and c . The black solid and dotted lines correspond to order τ^2 and c^2 , respectively. *Right*: Convergence of the limit approximation (25) in c . The black dotted line corresponds to the order c^{-1} .

References

- [1] Adams, R.A., Fournier, J.J.F., 2003. Sobolev spaces. volume 140 of *Pure and Applied Mathematics (Amsterdam)*. 2nd ed., Elsevier/Academic Press, Amsterdam.
- [2] Bao, W., Cai, Y., Jia, X., Tang, Q., 2016a. A uniformly accurate multiscale time integrator pseudospectral method for the Dirac equation in the nonrelativistic limit regime. *SIAM J. Numer. Anal.* 54, 1785–1812.
- [3] Bao, W., Cai, Y., Jia, X., Tang, Q., 2017. Numerical Methods and Comparison for the Dirac Equation in the Nonrelativistic Limit Regime. *J. Sci. Comput.* 71, 1094–1134.
- [4] Bao, W., Cai, Y., Jia, X., Yin, J., 2016b. Error estimates of numerical methods for the nonlinear Dirac equation in the nonrelativistic limit regime. *Sci. China Math.* 59, 1461–1494.
- [5] Bao, W., Li, X.G., 2004. An efficient and stable numerical method for the Maxwell-Dirac system. *J. Comput. Phys.* 199, 663–687.
- [6] Bechouche, P., Mauser, N.J., Poupaud, F., 1998. (Semi)-nonrelativistic limits of the Dirac equation with external time-dependent electromagnetic field. *Comm. Math. Phys.* 197, 405–425.
- [7] Bechouche, P., Mauser, N.J., Selberg, S., 2003. Derivation of Schrödinger Poisson as the non-relativistic limit of Klein-Gordon Maxwell, in: *Hyperbolic problems: theory, numerics, applications*. Springer, Berlin, pp. 357–367.
- [8] Bechouche, P., Mauser, N.J., Selberg, S., 2004. Nonrelativistic limit of Klein-Gordon-Maxwell to Schrödinger-Poisson. *Amer. J. Math.* 126, 31–64.
- [9] Bechouche, P., Mauser, N.J., Selberg, S., 2005. On the asymptotic analysis of the Dirac-Maxwell system in the nonrelativistic limit. *J. Hyperbolic Differ. Equ.* 2, 129–182.
- [10] Cai, Y., Wang, Y., 2018. A uniformly accurate (UA) multiscale time integrator pseudospectral method for the nonlinear Dirac equation in the nonrelativistic limit regime. *ESAIM Math. Model. Numer. Anal.* 52, 543–566.
- [11] Dirac, P.A.M., 1928. The quantum theory of the electron. *Proceedings of the Royal Society of London A: Mathematical, Physical and Engineering Sciences* 117, 610–624.
- [12] Faou, E., 2012. Geometric numerical integration and Schrödinger equations. *Zurich Lectures in Advanced Mathematics*, European Mathematical Society (EMS), Zürich.
- [13] Faou, E., Schratz, K., 2014. Asymptotic preserving schemes for the Klein-Gordon equation in the non-relativistic limit regime. *Numer. Math.* 126, 441–469.
- [14] Hairer, E., Lubich, C., Wanner, G., 2006. *Geometric numerical integration : structure-preserving algorithms for ordinary differential equations*. Springer series in computational mathematics ; 31. 2nd ed., Springer, Berlin.
- [15] Hörmander, L., 1997. *Lectures on nonlinear hyperbolic differential equations*. *Mathématiques & applications ; 26*, Springer, Berlin.
- [16] Huang, Z., Jin, S., Markowich, P.A., Sparber, C., Zheng, C., 2005. A time-splitting spectral scheme for the Maxwell-Dirac system. *J. Comput. Phys.* 208, 761–789.
- [17] Jahnke, T., Lubich, C., 2000. Error bounds for exponential operator splittings. *BIT* 40, 735–744.
- [18] Krämer, P., Schratz, K., 2017. Efficient time integration of the Maxwell-Klein-Gordon equation in the non-relativistic limit regime. *J. Comput. Appl. Math.* 316, 247–259.
- [19] Krämer, P., 2017. *Numerical Integrators for Maxwell-Klein-Gordon and Maxwell-Dirac Systems in Highly to Slowly Oscillatory Regimes*. Ph.D. thesis. Karlsruher Institut für Technologie (KIT).
- [20] Lemou, M., Méhats, F., Zhao, X., 2017. Uniformly accurate numerical schemes for the nonlinear Dirac equation in the nonrelativistic limit regime. *Commun. Math. Sci.* 15, 1107–1128.
- [21] Lubich, C., 2008a. From quantum to classical molecular dynamics: reduced models and numerical analysis. *Zurich Lectures in Advanced Mathematics*, European Mathematical Society (EMS), Zürich.
- [22] Lubich, C., 2008b. On splitting methods for Schrödinger-Poisson and cubic nonlinear Schrödinger equations. *Math. Comp.* 77, 2141–2153.
- [23] Masmoudi, N., Nakanishi, K., 2002. From nonlinear Klein-Gordon equation to a system of coupled nonlinear Schrödinger equations. *Math. Ann.* 324, 359–389.
- [24] Masmoudi, N., Nakanishi, K., 2003. Nonrelativistic limit from Maxwell-Klein-Gordon and Maxwell-Dirac to Poisson-Schrödinger. *Int. Math. Res. Not.* , 697–734.
- [25] Soler, M., 1970. Classical, stable, nonlinear spinor field with positive rest energy. *Phys. Rev. D* 1, 2766–2769.
- [26] Thaller, B., 1992. *The Dirac equation*. *Texts and monographs in physics*, Springer, Berlin.
- [27] Thirring, W.E., 1958. A soluble relativistic field theory. *Annals of Physics* 3, 91 – 112.